Journal of Non-Crystalline Solids 576 (2022) 121221

Contents lists available at ScienceDirect

Journal of Non-Crystalline Solids

journal homepage: www.elsevier.com/locate/jnoncrysol

Time-dependent deformation mechanism of metallic glass in different structural states at different temperatures

Nandita Ghodki, Maryam Sadeghilaridjani, Sundeep Mukherjee *

Department of Materials Science and Engineering, University of North Texas, Denton, TX 76203, USA

ARTICLE INFO

Keywords:
Creep
Nanoindentation
Stress exponent
Bulk metallic glass
Free volume
Shear transformation zone

ABSTRACT

There is limited understanding of time-dependent plastic deformation behavior of amorphous alloys as a function of their structural state. Here, the creep behavior of $Zr_{52.5}Ti_5Cu_{17.9}Ni_{14.6}Al_{10}$ bulk metallic glass was investigated in its as-cast and relaxed states using nanoindentation technique with applied load in the range of 500–1500 mN and temperature in the range of room temperature to 573 K. The creep displacement increased with increasing load and temperature since the creep process is thermally activated and diffusion rate is enhanced at elevated temperature and higher load. The creep strain rate sensitivity, which is a measure of the creep mechanism, increased with increase in temperature and decrease in applied load. This was attributed to the transition from localized to more homogeneous creep. Reduction in free volume for the relaxed alloy resulted in lower creep displacement and larger strain rate sensitivity compared to its as-cast counterpart. The results suggest that diffusion-based deformation dominate at higher temperature in contrast to shear transformation mediated plasticity at room temperature. The volume of shear transformation zone for the metallic glass was calculated using cooperative shearing model and correlated with the structural state for fundamental insights into the deformation process as a function of temperature and load.

1. Introduction

Bulk metallic glasses (BMGs) continue to attract widespread scientific and technological interest because of their unique thermoplastic processing ability and outstanding properties including ultra-high strength, large elastic strain limit, soft magnetic behavior and excellent corrosion resistance [1–10]. However, there are few reports and limited understanding of their time-dependent deformation behavior [11]. Lack of long-range atomic periodicity leads to a fundamentally different creep deformation mechanism for BMGs compared to crystalline metals/alloys and remains largely unexplored. In contrast to conventional bulk creep testing methods [12,13], nanoindentation creep technique has the advantages of small volume interrogation, rapid data acquisition, and non-destructive methodology. Creep behavior of BMGs has been studied previously using nanoindentation [14–16]; however, they are limited to low loads (<100 mN) and room temperature [17–22]. Du et al. studied the dynamic evolution of shear avalanches in metallic glasses using nanoindentation for explaining the plastic deformation behavior as a function of its structural state [14]. Huang et al. studied the room temperature nanoindentation creep behavior of an Fe-based [17] and Ti-based [18] BMG and showed more pronounced creep at higher loads and loading rates. Wei et al. studied the relaxation spectrum obtained from a generalized Kelvin model for Ce-based bulk metallic glasses [19]. Nanoindentation creep of Cu-Zr [20] and Zr-based [21] metallic glass thin films was investigated to understand the effect of applied strain rates and indentation depth on the creep deformation mechanisms. Xu et al. showed loading rate sensitivity for an Fe-based BMG and discussed the creep mechanism in the context of free volume and shear transformation zones [22]. However, time-dependent deformation of BMGs at high temperatures have not been reported, particularly at high loads thereby eliminating possible surface effects. In addition, the influence of structural state of the metallic glass (obtained by different processing conditions) on its creep behavior is not well understood. Structural relaxation typically leads to embrittlement of metallic glasses causing a reduction in its ductility and fracture toughness [[23],[24]]. In contrast, thermal rejuvenation by cryogenic cycling has been shown to improve the ductility of metallic glasses and promote plasticization by introducing defects and excess free volume [25–27]. However, the time-dependent deformation behavior of metallic glasses in different structural states has not been investigated in detail.

* Corresponding author.
E-mail address: sundeep.mukherjee@unt.edu (S. Mukherjee).

https://doi.org/10.1016/j.jnoncrysol.2021.121221
Received 1 September 2021; Received in revised form 6 October 2021; Accepted 7 October 2021

Here, the creep response of $Zr_{52.5}Ti_5Cu_{17.9}Ni_{14.6}Al_{10}$ bulk metallic glass was studied using nanoindentation technique in the range of room temperature to 573 K and applied load ranging from 500 to 1500 mN. This particular BMG was chosen as a model alloy system for the time-dependent deformation study because of its excellent glass forming ability, thermal stability, absence of toxic constituents (such as Be), and potential for commercial use [28]. The underlying creep mechanism, as a function of load and temperature, is discussed in the context of free volume and shear transformation mediated deformation in the as-cast versus relaxed state of the BMG.

2. Experimental

Zr-based bulk metallic glass with composition of $Zr_{52.5}Ti_5Cu_{17.9}Ni_{14.6}Al_{10}$ was prepared using arc melting followed by suction casting. The sample was annealed at 630 K for 30 min to achieve sufficient relaxation, as reported previously [28]. The as-cast and relaxed samples were mechanically polished to a mirror finish and then cleaned in acetone and distilled water ultrasonically for 15 min for nano-mechanical tests. Rigaku III Ultima X-ray diffractometer (XRD, Rigaku Corporation, Tokyo, Japan) with 1.54 Å wavelength Cu-Kα radiation was used to confirm the amorphous structure of the samples and the characteristic temperatures and enthalpies were determined by differential scanning calorimetry (DSC) analysis (NETZSCH DSC 404C).

Nanoindentation creep tests were performed using TI-Premier Triboindenter (Bruker, Minneapolis, MN, USA) with a Sapphire Berkovich tip having an included angle of 142.30°, tip radius of 150 nm, and integrated with XSol600 heating stage for heating the samples up to 873 K. The instrument resolution in terms of load was 1 nN, in terms of displacement was 0.006 nm, and temperature accuracy was within 0.001 °C. Fused quartz was used as a standard reference sample for initial tip calibration. The tests were carried out in Ar + 5% H_2 gas environment to prevent oxidation. Static creep tests were performed under constant load at room temperature, 423 and 573 K. The tests were done by ramping to a maximum load of 500, 1000 and 1500 mN at a high loading rate of 20 mN/s and then held for 600 s at the maximum load followed by unloading. High load was used to minimize surface effects and avoid indentation size effect (ISE) on hardness. A high loading rate was chosen to ensure that creep primarily occurred during the dwell time. At least fifteen indents were performed in each test condition and the distance between two neighboring indents was kept greater than 100 μm to avoid the overlap of their plastic zones. At elevated temperature, the sample was held at the prescribed set point for at least 20 min to reach steady state and the indenter tip was maintained close to the sample to reduce temperature gradient. Triboindenter software was used to correct thermal drift, which was ~0.05–0.1 nm/s.

3. Results

Specific heat as a function of temperature obtained using DSC for $Zr_{52.5}Ti_5Cu_{17.9}Ni_{14.6}Al_{10}$ BMG in as-cast and relaxed conditions are shown in Fig. 1(a). The glass transition temperature (*Tg*) for the as-cast sample was ~683 K and crystallization temperature (*Tx*) was ~728 K, suggesting a wide super-cooled liquid region ($\Delta T = 45$ K). The *Tg* and *Tx* of the relaxed sample were very similar to the as-cast alloy (*Tg* ~ 680 K and *Tx* ~ 726 K). An exothermic peak was observed just after the glass transition, which is a measure of the relaxation enthalpy due to the annihilation of excess free volume [23]. This excess enthalpy is shown by the shaded region of the DSC curves after the glass transition for the as-cast and relaxed BMGs in the insets, Fig. 1(a1,a2). Based on free volume theory, the equilibrium free volume (v_f) as a function of temperature (T) is given by the relation [29–31]:

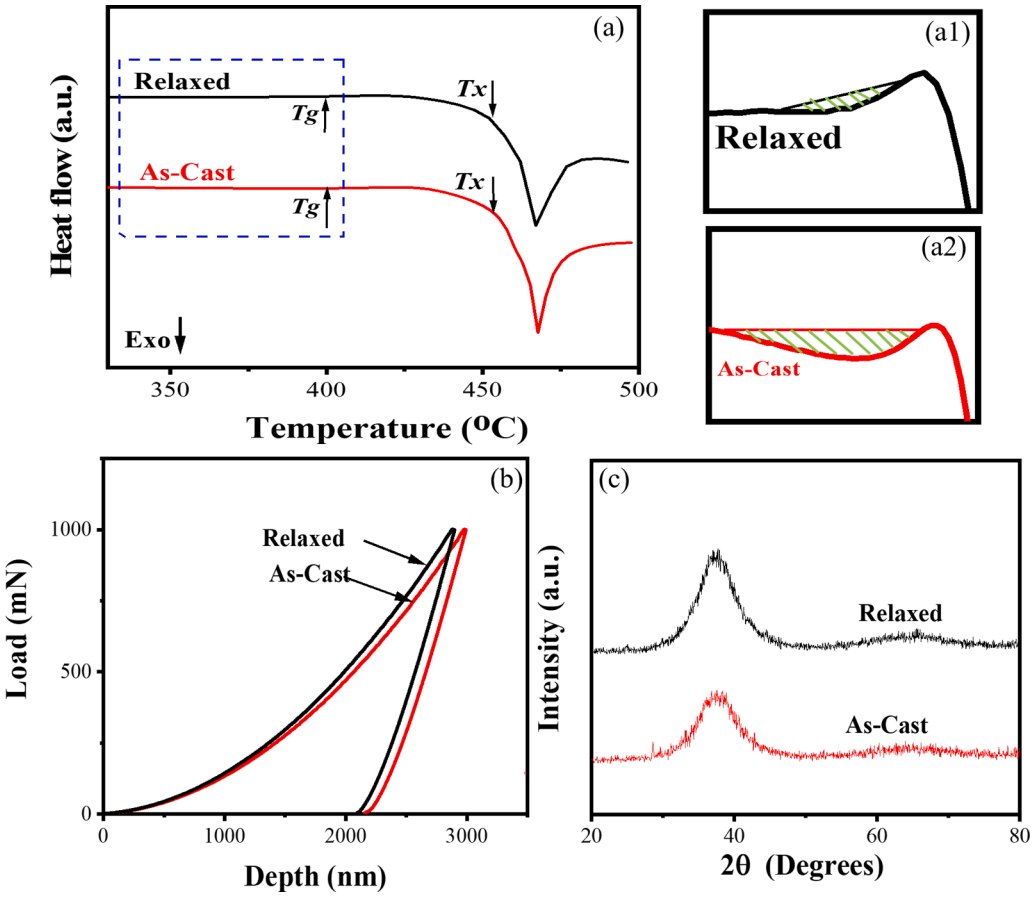

Fig. 1. (a) DSC plots for as-cast and relaxed BMG showing Tg and Tx; (a1) and (a2) show zoomed-in view around glass transition region indicating lower relaxation enthalpy for relaxed sample compared to as-cast; (b) nano-indentation load-depth curves for as-cast and relaxed BMG at 1000 mN peak load showing lower indentation depth for relaxed BMG suggesting an increase in hardness upon relaxation; (c) XRD pattern of as-cast and relaxed samples showing amorphous structure for both.

$$\upsilon_f = A(T - T_0) \quad (1)$$

where, T_0 is the ideal glass transition temperature and A is a proportionality constant. The excess free volume created due to non-equilibrium processing in the as-cast BMG gets annihilated during continuous heating in DSC. This reduction in free volume results in heat release in the form of enthalpy of relaxation (ΔH_{relax}), which is directly proportional to the excess free volume of the BMG [32]. ΔH_{relax} decreased by almost an order of magnitude from 0.037 J/g for the as-cast alloy to 0.0039 J/g for the relaxed alloy. The lower enthalpy of relaxation for the relaxed sample indicates annihilation of free volume from the sub-*Tg* annealing. Nanoindentation load-depth curves at 1000 mN for the as-cast and relaxed BMG are shown in Fig. 1(b). The reduction in indentation depth for the relaxed sample suggests an increase in the hardness value of the BMG upon sub-*Tg* annealing. The hardness of the as-cast and relaxed BMG was measured using Oliver and Pharr method [33]. As-cast BMG showed a hardness value of 5.6 ± 0.03 GPa and reduced modulus of 108.2 ± 0.37 GPa. The hardness and modulus for the relaxed BMG increased to 6.0 ± 0.03 GPa and 113.3 ± 0.38 GPa, respectively. The increase in hardness as well as modulus for the relaxed sample shows that sub-*Tg* annealing resulted in denser packing of atoms and reduction in free volume. Fig. 1(c) shows XRD patterns obtained for the as cast and relaxed $Zr_{52.5}Ti_5Cu_{17.9}Ni_{14.6}Al_{10}$ BMG indicating broad diffraction peaks and supporting the fully amorphous structure for both the samples.

Fig. 2(a) shows the typical load-depth (*P-h*) curves for as-cast $Zr_{52.5}Ti_5Cu_{17.9}Ni_{14.6}Al_{10}$ obtained from the nanoindentation creep tests as a function of temperature (298, 423, 573 K) at peak load of 1000 mN. The origin of each curve has been offset for clarity. Fig. 2(b) is a zoomed-in view of Fig. 2(a) showing a clear difference in serration behavior as a function of temperature. Similar serration behavior was observed for the relaxed alloy as well and the corresponding load-depth curves are shown in Supplementary Fig. S1(a,b). Fig. 2(c) shows the serration length versus temperature for both the alloys, indicating an increase in serration length with increase in temperature for both as-cast and relaxed $Zr_{52.5}Ti_5Cu_{17.9}Ni_{14.6}Al_{10}$. The magnitude and number of "pop-ins" in the loading curves were higher at 573 K compared to lower temperatures in agreement with previous reports [34]. Serrated flow is associated with shear band nucleation in metallic glasses to accommodate plastic strain [35]. BMGs show greater resistance to shear banding at high temperatures leading to more serrated flow [34]. At higher temperatures, greater diffusion in the bulk results in larger strains for shear band propagation and consequently larger "pop-ins" due to low propensity for shear localization [1]. Shear strain accommodation in a single shear band reduces at low temperature to almost half of that accommodated at high temperature [34]. This suggests that as many as twice the number of shear bands may be accommodated at lower temperature with smaller spacing resulting in less serrations. The relaxed sample showed slightly higher serration length at all temperatures as compared to the as-cast alloy, which may be attributed to less free volume in the relaxed sample that allows a smaller number of shear bands to accommodate the strain. To reduce or eliminate the effect of free volume changes during measurement, the hardness and reduced modulus of the relaxed $Zr_{52.5}Ti_5Cu_{17.9}Ni_{14.6}Al_{10}$ was determined as a function of temperature, as shown in Fig. 2(d). The hardness decreased by ~20% and modulus decreased by ~40% with increase in

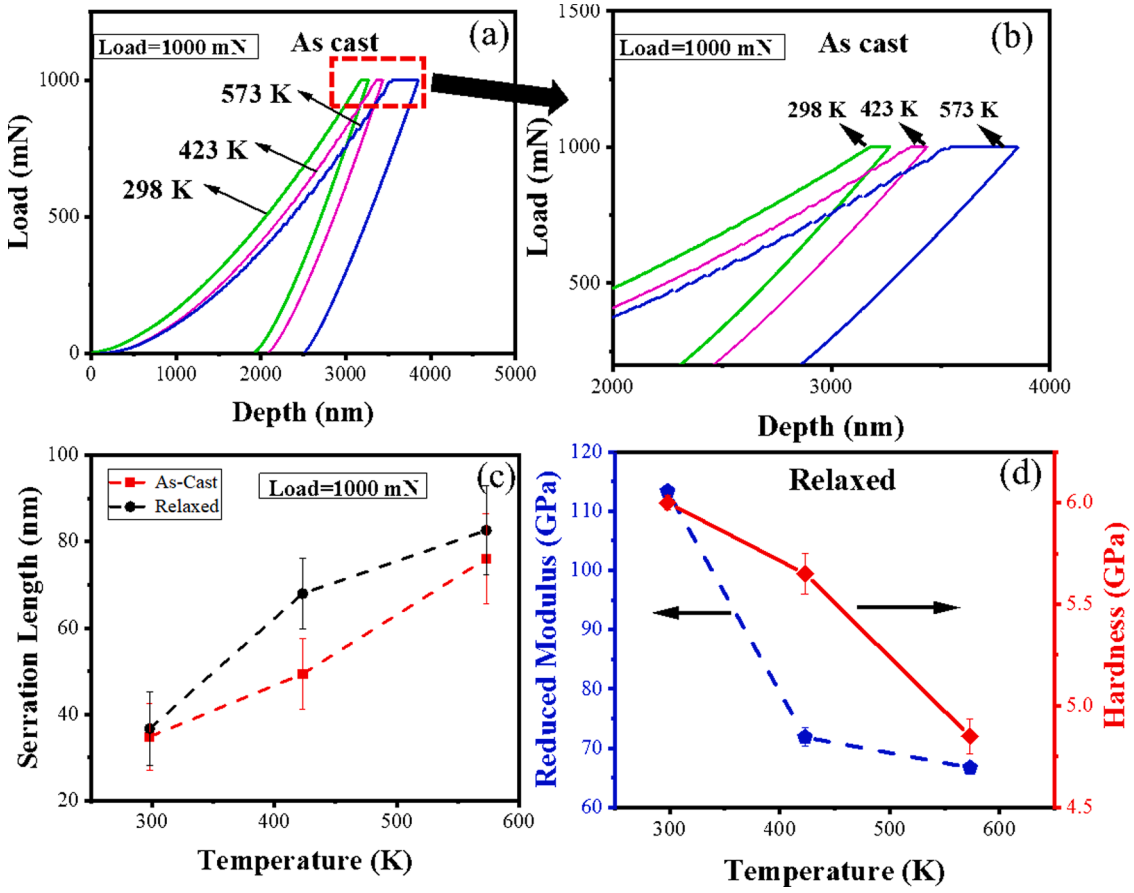

Fig. 2. (a) Typical nanoindentation load-depth plot for as-cast $Zr_{52.5}Ti_5Cu_{17.9}Ni_{14.6}Al_{10}$ as a function of temperature; (b) zoomed-in view of selected part in (a) showing change in serration behavior of as-cast $Zr_{52.5}Ti_5Cu_{17.9}Ni_{14.6}Al_{10}$ as a function of temperature; (c) serration length as a function of temperature for as-cast and relaxed $Zr_{52.5}Ti_5Cu_{17.9}Ni_{14.6}Al_{10}$ showing increase in serration length with temperature increase; (d) hardness and modulus of relaxed $Zr_{52.5}Ti_5Cu_{17.9}Ni_{14.6}Al_{10}$ as a function of temperature.

temperature from room temperature to 573 K, indicating a sharp reduction in "equilibrium" strength and stiffness over this temperature range, which is well below the glass transition temperature of ~680 K.

Fig. 3(a,b) show the creep displacement as a function of the holding time at the three temperatures of 298 K, 423 K, and 573 K, for the as-cast and relaxed BMG, respectively. Nanoindentation creep tests involve non-homogeneous and complex stress state that are distinctly different from uniaxial creep tests. The instantaneous stress generated during nanoindentation creep decreases with holding time and the creep rate approaches a steady state value towards the end of holding time (as seen in Fig. 3(a,b)). Maximum creep displacement as a function of load and temperature for as-cast and relaxed BMG are shown in Fig. 3(c,d), respectively. Each data point is an average of 15 indents. The maximum creep displacement increased with peak load and temperature since the creep process is thermally activated and diffusion rate is enhanced at elevated temperature and higher load. Increasing peak load enhanced free volume generation rate resulting in more pronounced creep deformation during holding time [17,36]. The as-cast sample showed larger

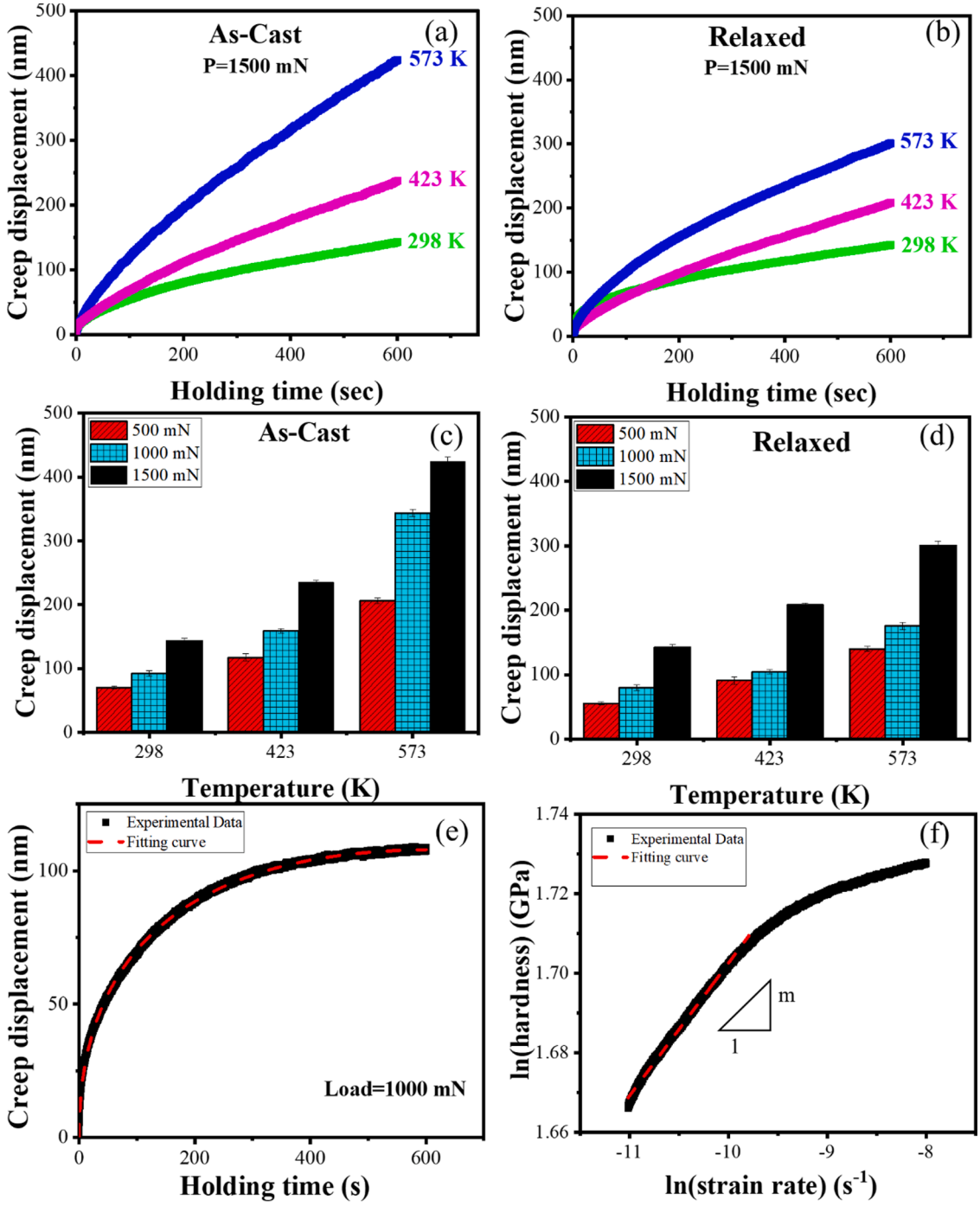

Fig. 3. Creep displacement versus holding time at the temperatures of 298, 423 and 573 K for: (a) as-cast and (b) relaxed $Zr_{52.5}Ti_5Cu_{17.9}Ni_{14.6}Al_{10}$ BMG; maximum creep displacement as a function of load and temperature for: (c) as-cast and (d) relaxed $Zr_{52.5}Ti_5Cu_{17.9}Ni_{14.6}Al_{10}$ BMG, indicating that the creep displacement increased with increase in load and temperature; (e) Creep displacement versus holding time, with experimental results shown by black data points and empirical fit (Eq. (4)) shown by red dashed line; (f) log–log plot of hardness versus strain rate to obtain creep strain rate sensitivity (m) by linear fitting of the steady-state part (For interpretation of the references to color in this figure legend, the reader is referred to the web version of this article.).

creep displacement as compared to the relaxed alloy for all the loads and temperatures studied due to its higher free volume fraction leading to more pronounced time-dependent plastic deformation. Further investigation of high temperature creep mechanism for the BMG was done by evaluating the stress exponent (n), defined in the conventional power-law creep as [37]:

$$\dot{\varepsilon} = A\sigma^n = A^{'}H^n \tag{2}$$

where, $\dot{\varepsilon}$ is the strain rate, σ is the applied stress, A *or* $A^{'}$ is a temperature-dependent material constant, and H is the hardness. The strain rate $(\dot{\varepsilon})$ was calculated as:

$$\dot{\varepsilon} = \frac{1}{h}\frac{dh}{dt} \tag{3}$$

where, $\frac{dh}{dt}$ is the first derivative of the instantaneous creep displacement (h). The displacement rate dh/dt was obtained by fitting the displacement-holding time curve as [38]:

$$h\ (t) = h_0 + a(t - t_0)^p + kt \tag{4}$$

where, h_0 and t_0 are the indentation depth and time before the holding segment, and a, p, and k are fitting constants. The representative fitting curve is shown in Fig. 3(e) with correlation coefficient $R^2 > 0.997$. The fitting parameters for all the conditions are summarized in supplementary Table S1. Hardness (H) measured using a self-similar indentation probe like Berkovich was calculated as:

$$H = \frac{P}{24.5\ h_c^2} \tag{5}$$

where, P is the applied load, h_c is the contact depth given by $h_c = h_{max} - 0.75\ P/S$ for Berkovich indenter and h_{max} and S are maximum penetration depth and material stiffness, respectively. Slope of log (H) versus log $(\dot{\varepsilon})$ at steady state was used to calculate the creep strain rate sensitivity (m), which is the reciprocal of stress exponent, as shown in Fig. 3 (f).

4. Discussion

Unlike in crystalline metals, plastic flow in amorphous alloys is mediated through shear transformation zones [35], where a small cluster of atoms spontaneously and cooperatively reorganize under the action of applied shear stress [34,39–41]. The creep strain rate sensitivity for a BMG is a measure of its tendency for flow localization while undergoing mechanical deformation. Large strain rate sensitivity and smaller values of stress exponent indicate high resistance to localization during plastic deformation [42]. The dependence of creep strain rate sensitivity on load and temperature for the as-cast and relaxed BMG is shown in Fig. 4(a). Creep strain rate sensitivity decreased with increase in applied load and increased with temperature, being higher by almost an order of magnitude at 573 K compared to room temperature. Fig. 4(b) shows the corresponding STZ volume at different temperatures and peak loads. STZ volume provides valuable insights into the microscopic

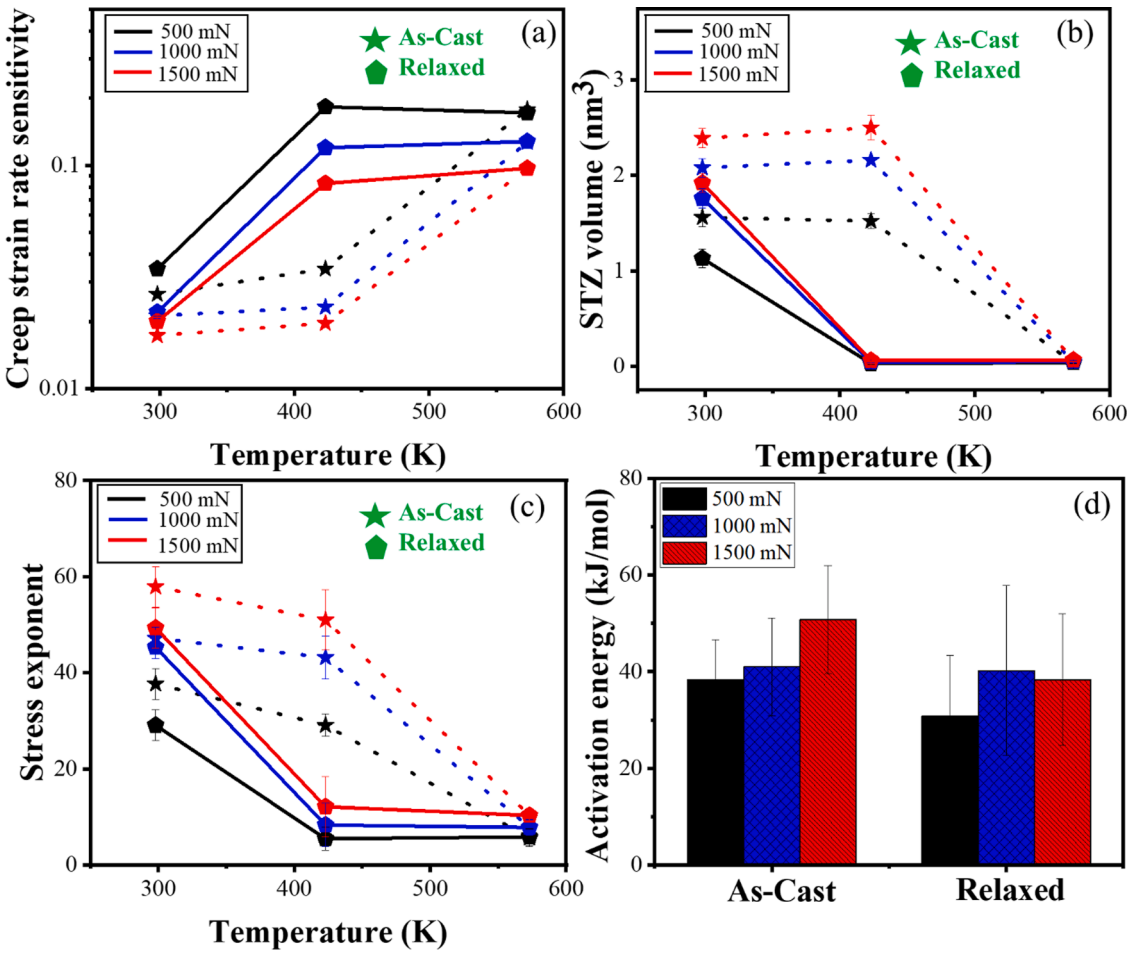

Fig. 4. (a) Creep strain rate sensitivity at different loads as a function of temperature for as-cast and relaxed $Zr_{52.5}Ti_5Cu_{17.9}Ni_{14.6}Al_{10}$ BMG; (b) the STZ volume calculated at various loads and temperatures for as-cast and relaxed BMG; (c) creep stress exponent at different loads as a function of temperature for as cast and relaxed $Zr_{52.5}Ti_5Cu_{17.9}Ni_{14.6}Al_{10}$ BMG; (d) activation energy at different loads for as-cast and relaxed $Zr_{52.5}Ti_5Cu_{17.9}Ni_{14.6}Al_{10}$ BMG.

mechanism of plasticity in BMGs and the values obtained here are in the same range as reported previously in experimental studies [43] as well as by computation [44]. STZs generally consist of a few atoms to a few hundred atoms [44]. In amorphous alloys, there is competition between STZ initiation and atomic diffusion depending on the temperature and applied strain rate [1]. The STZ volume was calculated based on the Johnson-Sawmer cooperative shearing model [39,43] by correlating inelastic strain rate ($\dot{\gamma}$) with dynamical state variables as [39]:

$$\dot{\gamma} = \dot{\gamma}_0 \exp(-W^* / kT) \tag{6}$$

where, $\dot{\gamma}_0$ is a constant at 0 K, k is Boltzmann constant, T is the absolute temperature and W^* is the activation energy given as [33]:

$$W^* = 4R_0 G_0 {\gamma_c}^2 \left(1 - \frac{\tau}{\tau_c}\right)^{3/2} \Omega\xi \tag{7}$$

where, Ω is the volume of STZ, G_0 and τ_c are shear modulus and threshold shear resistance of metallic glass at 0 K, respectively. R_0 and ξ are constants with approximate values of 0.5 and 3, respectively [43] and γ_c is the approximate elastic limit for BMGs which is ~0.027 [[43], [44]]. The STZ activation energy correlates with the redistribution of atoms in a dispersed volume under external load. STZ volume may be calculated in terms of hardness and creep strain-rate sensitivity (m) as [43]:

$$\Omega = \left(\frac{kT\sqrt{3}}{2G_0{\gamma_c}^2}\right) \frac{1}{R_0\xi} \frac{1}{m\left(\frac{H}{\tau_c}\right)\left(1 - \frac{\tau_{CT}}{\tau_c}\right)^{\frac{1}{2}}} \tag{8}$$

where, τ_{CT} is threshold shear resistance at temperature T [43]. The as-cast sample showed almost an order of magnitude higher excess free volume compared to its relaxed state (DSC plot in Fig. 1(a)). At 423 K, the fraction of free volume annihilated for the as-cast sample is likely to be significantly smaller compared to that of the relaxed sample. This is evident from the negligible change in STZ volume for the as-cast sample compared to the large change for its relaxed counterpart (Fig. 4(b)). With further increase in temperature to 573 K, the free volume was rapidly annihilated for the as-cast sample, and it approached values similar to the relaxed sample resulting in comparable STZ volumes for both the states as seen in Fig. 4(b). The dependence of stress exponent on load and temperature for the as-cast and relaxed BMG is shown in Fig. 4 (c). A smaller value of stress exponent is associated with homogeneous plastic deformation of the material. Creep stress exponent decreased with decrease in applied load and increase in temperature. At room temperature, the stress exponent value increased by ~50% with increase in load from 500 mN to 1500 mN, indicating a significant dependence on load (Fig. 4(c)). The stress exponent value was high at room temperature indicating inhomogeneous plastic deformation and decreased sharply to lower values at higher temperatures suggesting a transition to more homogeneous plastic flow for both the as-cast and relaxed BMGs [45, 46]. Fig. 4(d) shows the activation energy for the as-cast and relaxed BMG at different loads. Temperature dependence of the indentation creep rate may be represented by a power-law as [47]:

$$\dot{\varepsilon} = A\sigma^n \exp\left(-\frac{Q}{RT}\right) \approx AH^n \exp\left(-\frac{Q}{RT}\right) \tag{9}$$

where, A is a structure dependent constant, H is the hardness, R is the universal gas constant, and Q is the activation energy. The slope of ln $(\dot{\varepsilon}/H^n)$ versus 1000/T was used to calculate the activation energy (Q) for the as-cast and relaxed BMG. An average of strain rate and hardness in the constant load region was selected for analysis at each temperature and the creep activation energy was obtained by linear regression fitting. The activation energy obtained from bulk creep tests have been reported to be in the range of ~100–500 kJ/mol [11]. However, our values of activation energy obtained from nanoindentation creep are lower (Fig. 4(d)). This may be because of the smaller affected volume and large strain gradients during the small-scale nanoindentation tests. In addition, the higher activation energy for the as-cast BMG compared to its relaxed state may be attributed to the presence of more free volume and associated larger STZ volume.

At smaller indentation depth (i.e., lower load), a large strain gradient is expected [22,48] and the STZs are likely to be small due to the confined volume. The STZs become unstable as a result of the strain gradient beneath the indenter and speed up the rate of shear band formation [49]. Thus, constrained volume results in a large strain gradient and activates smaller STZs to flow in a more homogeneous manner as illustrated in the schematic shown in Fig. 5(a). At larger applied loads, the volume beneath the indenter is more, which results in larger STZ volume (Fig. 4(b)) and more localized flow behavior as evident from lower creep strain rate sensitivity (Fig. 4(a)). The difference in STZ volume as a function of load decreased with increase in temperature possibly because high-temperature diffusion processes overshadow the effect of load. The rate of diffusion of atoms to form and dissolve the STZs may become very high at high temperatures, thus enabling homogeneous plastic flow as compared to lower temperature where localized plastic flow is evident from the lower strain rate sensitivity value. As shown in Fig. 4(b), the STZ volume decreased from ~ 2.4 nm^3 to 0.036 nm^3 for the as-cast BMG and from ~1.92 nm^3 to 0.027 nm^3 for relaxed BMG with increase from room temperature to 573 K. Increased thermal energy at high temperatures reduces the diffusion barrier for atoms leading to more diffusion dominated plastic deformation [43]. This is illustrated in schematic Fig. 5(b), with the sample at higher temperature exhibiting more diffusion dominant plastic deformation as compared to STZ mediated plastic deformation at room temperature. At high temperatures, diffusion of atoms prevents localization, thus requiring larger strains for flow to occur as was confirmed with more serrated flow in the load-depth (P-h) curves in Fig. 2(b). Prior studies have reported on the correlation between STZ volume and BMG structural state using nanoindentation rate-change tests [42,50]. Fig. 4(a) shows that the relaxed BMG with lower amount of free volume [51] has higher creep strain rate sensitivity than the as-cast BMG, particularly at low temperatures. Higher free volume promotes more STZ initiation and corresponding shear band formation because of easier atomic rearrangement. Since the relaxed BMG possesses comparatively less free volume than the as-cast BMG, it has less volume fraction of atoms involved in cooperative shearing as illustrated in the schematic Fig. 5(c), with the difference being particularly notable at the intermediate temperatures (Fig. 4(b)).

5. Conclusion

In summary, creep behavior of $Zr_{52.5}Ti_5Cu_{17.9}Ni_{14.6}Al_{10}$ bulk metallic glass was investigated using nanoindentation as a function of applied load, temperature, and structural state of the glass. At the high temperature of 573 K, the creep strain rate sensitivity increased sharply and did not depend on the load indicating that diffusion processes overshadowed the effect of load. The STZ volume increased with load due to lower strain gradient suggesting STZ dominance in creep deformation, whereas it decreased with increasing temperature supporting diffusion controlled plastic flow at higher temperatures. The reduction in free volume of sub-Tg annealed $Zr_{52.5}Ti_5Cu_{17.9}Ni_{14.6}Al_{10}$ bulk metallic glass led to its smaller creep displacement, higher creep strain rate sensitivity, and smaller STZ volume compared to the corresponding as-cast state. This study provides insights into the STZ volume for metallic glasses in different structural states, with drastic change in the underlying mechanisms of time-dependent plastic deformation as a function of temperature.

Data availability

The data that supports the findings of this study are available within the article and its supplementary material.

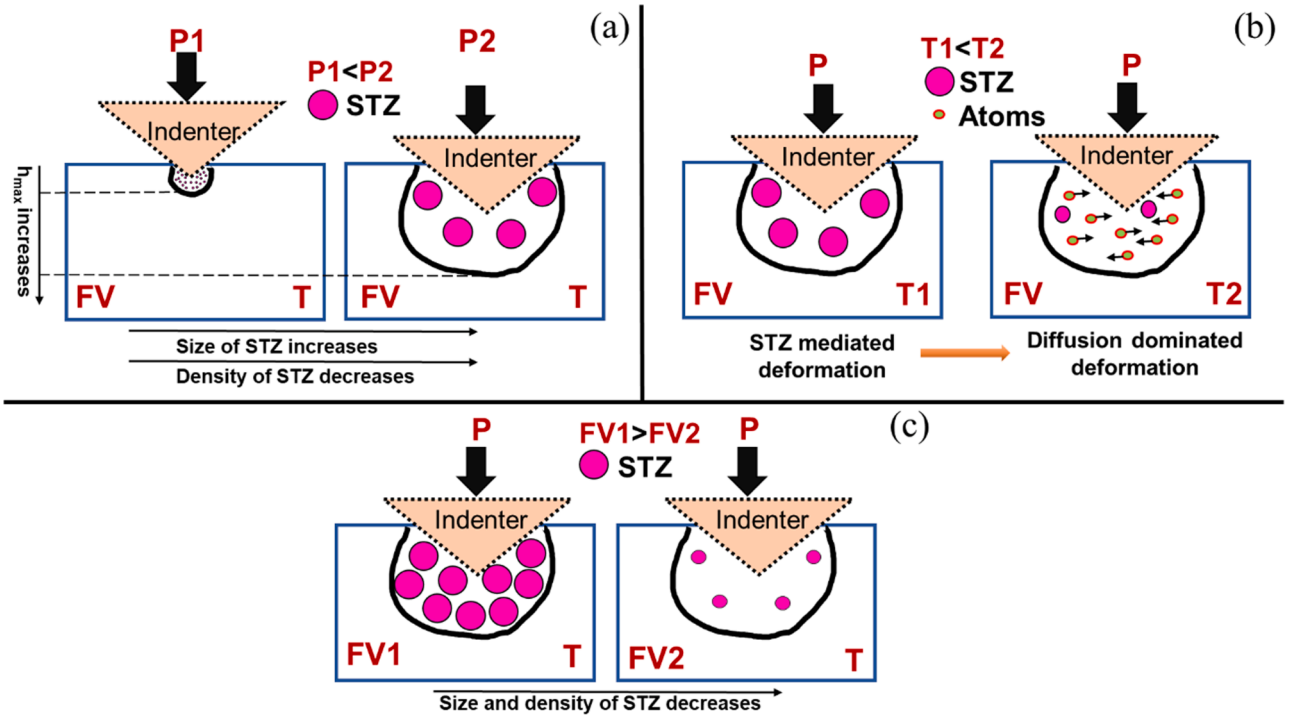

Fig. 5. Schematic illustration of STZ nucleation underneath the nanoindenter probe as a function of: (a) load (at constant free volume and temperature), (b) temperature (at constant free volume and load), and (c) free volume (at constant load and temperature).

CRediT authorship contribution statement

Nandita Ghodki: Conceptualization, Formal analysis, Investigation, Writing – original draft. **Maryam Sadeghilaridjani:** Investigation, Writing – original draft. **Sundeep Mukherjee:** Conceptualization, Investigation, Resources, Supervision, Project administration, Writing – review & editing.

Declaration of Competing Interest

The authors declare that they have no conflict of interest that could have appeared to influence the work reported in this paper.

Acknowledgments

This work was partly supported by funding from the National Science Foundation (NSF) under Grant No. 1762545. Any opinions, findings, and conclusions expressed in this paper are those of the authors and do not necessarily reflect the views of the National Science Foundation (NSF). The authors also acknowledge the Materials Research Facility (MRF) at University of North Texas for some of the characterization used in this study.

Supplementary materials

Supplementary material associated with this article can be found, in the online version, at doi:10.1016/j.jnoncrysol.2021.121221. Supplementary Fig. S1(a,b) for the serration behavior in relaxed $Zr_{52.5}Ti_{5}Cu_{17.9}Ni_{14.6}Al_{10}$ BMG and supplementary Table S1 for the fitting parameters of the displacement-holding time curves.

References

[1] C.A. Schuh, T.C. Hufnagel, U. Ramamurty, Mechanical behavior of amorphous alloys, Acta Mater. 55 (2007) 4067–4109, https://doi.org/10.1016/j.actamat.2007.01.052.
[2] H.S. Arora, H.S. Grewal, H. Singh, S. Mukherjee, Zirconium based bulk metallic glass-Better resistance to slurry erosion compared to hydroturbine steel, Wear 307 (1–2) (2013) 28–34, https://doi.org/10.1016/j.wear.2013.08.016.
[3] S. Das, S. Garrison, S. Mukherjee, M.D. Baró, J. Sort, Bi-Functional mechanism in degradation of toxic water pollutants by catalytic amorphous metals, Advanced Engineering Materials 18 (2) (2015) 214–218, https://doi.org/10.1002/adem.201500239.
[4] H.S. Arora, Q. Xu, Z. Xia, Y.H. Ho, N.B. Dahotre, J. Schroers, S. Mukherjee, Wettability of nanotextured metallic glass surfaces, Scripta Materialia 69 (10) (2013) 732–735, https://doi.org/10.1016/j.scriptamat.2013.08.014.
[5] C. Suryanarayana, A. Inoue, Bulk Metallic Glasses, CRC Press, Boca Raton, FL, 2011.
[6] W.H. Wang, Bulk metallic glasses with functional physical properties, Adv. Mater. 21 (2009) 4524–4544, https://doi.org/10.1002/adma.200901053.
[7] P. Meagher, E.D. O'Cearbhaill, J.H. Byrne, D.J. Browne, Bulk metallic glasses for implantable medical devices and surgical tools, Adv. Mater. 28 (2016) 5755–5762, https://doi.org/10.1002/adma.201505347.
[8] A. Inoue, A. Takeuchi, Recent development and application products of bulk glassy alloys, Acta Mater. 59 (2011) 2243–2267, https://doi.org/10.1016/j.actamat.2010.11.027.
[9] H.F. Li, Y.F. Zheng, Recent advances in bulk metallic glasses for biomedical applications, Acta Biomater. 36 (2016) 1–20, https://doi.org/10.1016/j.actbio.2016.03.047.
[10] Z. Shao, M. Gopinadhan, G. Kumar, S. Mukherjee, Y. Liu, C.S. O`Hern, J. Schroers, C.S. Osuji, Size-dependent viscosity in the super-cooled liquid state of a bulk metallic glass, Applied Physics Letters 102 (221901) (2013), https://doi.org/10.1063/1.4808342.
[11] M.E. Kassner, K. Smith, V. Eliasson, Creep in amorphous metals, J. Mater. Res. Technol. 4 (2015) 100–107, https://doi.org/10.1016/j.jmrt.2014.11.003.
[12] J.C. Qiao, J.M. Pelletier, Y. Yao, Creep in bulk metallic glasses. Transition from linear to non linear regime, Mater. Sci. Eng. A. 743 (2019) 185–189, https://doi.org/10.1016/j.msea.2018.11.066.
[13] B.S.S. Daniel, A. Reger-Leonhard, M. Heilmaier, J. Eckert, L. Schultz, Thermal relaxation and high temperature creep of Zr55Cu30Al10Ni5 bulk metallic glass, Mech. Time Depend. Mater. 6 (2002) 193–206, https://doi.org/10.1023/A:1015045324786.
[14] Y. Du, Q. Zhou, Q. Jia, Y. Shi, H. Wang, J. Wang, Imparities of shear avalanches dynamic evolution in a metallic glass, Mater. Res. Lett. 8 (2020) 357–363, https://doi.org/10.1080/21663831.2020.1771450.
[15] Q. Zhou, W. Han, D. Luo, Y. Du, J. Xie, X.Z. Wang, Q. Zou, X. Zhao, H. Wang, B. D. Beake, Mechanical and tribological properties of Zr–Cu–Ni–Al bulk metallic glasses with dual-phase structure, Wear 474–475 (2021), 203880, https://doi.org/10.1016/j.wear.2021.203880.
[16] D. Hua, Q. Xia, W. Wang, Q. Zhou, S. Li, D. Qian, J. Shi, H. Wang, Atomistic insights into the deformation mechanism of a CoCrNi medium entropy alloy under nanoindentation, Int. J. Plast. 142 (2021), 102997, https://doi.org/10.1016/j.ijplas.2021.102997.

[17] Y.J. Huang, J. Shen, Y.L. Chiu, J.J.J. Chen, J.F. Sun, Indentation creep of an Fe-based bulk metallic glass, Intermetallics 17 (2009) 190–194, https://doi.org/10.1016/j.intermet.2008.09.014.
[18] Y.J. Huang, Y.L. Chiu, J. Shen, J.J.J. Chen, J.F. Sun, Indentation creep of a Ti-based metallic glass, J. Mater. Res. 24 (2009) 993–997, https://doi.org/10.1557/JMR.2009.0119.
[19] B. Wei, T. Zhang, W. Li, D. Xing, L. Zhang, Y. Wang, Indentation creep behavior in Ce-based bulk metallic glasses at room temperature, Mater. Trans. 46 (2005) 2959–2962, https://doi.org/10.2320/matertrans.46.2959.
[20] Y. Wang, J. Zhang, K. Wu, G. Liu, D. Kiener, J. Sun, Nanoindentation creep behavior of Cu–Zr metallic glass films, Mater. Res. Lett. 6 (2018) 22–28, https://doi.org/10.1080/21663831.2017.1383946.
[21] F. Wang, J.M. Li, P. Huang, W.L. Wang, T.J. Lu, K.W. Xu, Nanoscale creep deformation in Zr-based metallic glass, Intermetallics 38 (2013) 156–160, https://doi.org/10.1016/j.intermet.2013.03.006.
[22] F. Xu, Z.L. Long, X.H. Deng, P. Zhang, Loading rate sensitivity of nanoindentation creep behavior in a Fe-based bulk metallic glass, Trans. Nonferr. Met. Soc. China 23 (2013) 1646–1651, https://doi.org/10.1016/S1003-6326(13)62643-6 (English Ed.
[23] P. Murali, U. Ramamurty, Embrittlement of a bulk metallic glass due to sub-Tg annealing, Acta Mater. 53 (2005) 1467–1478, https://doi.org/10.1016/j.actamat.2004.11.040.
[24] U. Ramamurty, M.L. Lee, J. Basu, Y. Li, Embrittlement of a bulk metallic glass due to low-temperature annealing, Scr. Mater. 47 (2002) 107–111, https://doi.org/10.1016/S1359-6462(02)00102-1.
[25] W. Guo, R. Yamada, J. Saida, S. Lü, S. Wu, Various rejuvenation behaviors of Zr-based metallic glass by cryogenic cycling treatment with different casting temperatures, Nanoscale Res. Lett. (2018) 13, https://doi.org/10.1186/s11671-018-2816-7.
[26] J. Pan, Y.X. Wang, Q. Guo, D. Zhang, A.L. Greer, Y. Li, Extreme rejuvenation and softening in a bulk metallic glass, Nat. Commun. 9 (2018), https://doi.org/10.1038/s41467-018-02943-4.
[27] W. Guo, R. Yamada, J. Saida, Rejuvenation and plasticization of metallic glass by deep cryogenic cycling treatment, Intermetallics 93 (2018) 141–147, https://doi.org/10.1016/j.intermet.2017.11.015.
[28] W. Dmowski, C. Fan, M.L. Morrison, P.K. Liaw, T. Egami, Structural changes in bulk metallic glass after annealing below the glass-transition temperature, Mater. Sci. Eng. A. 471 (2007) 125–129, https://doi.org/10.1016/j.msea.2006.12.137.
[29] M. Heggen, F. Spaepen, M. Feuerbacher, Creation and annihilation of free volume during homogeneous flow of a metallic glass, J. Appl. Phys. (2005) 97, https://doi.org/10.1063/1.1827344.
[30] A. van den Beukel, J. Sietsma, The glass transition as a free volume related kinetic phenomenon, Acta Metall. Mater. 38 (1990) 383–389, https://doi.org/10.1016/0956-7151(90)90142-4.
[31] D. Turnbull, M.H. Cohen, On the free-volume model of the liquid-glass transition, J. Chem. Phys. 52 (1970) 3038–3041, https://doi.org/10.1063/1.1673434.
[32] A. Slipenyuk, J. Eckert, Correlation between enthalpy change and free volume reduction during structural relaxation of Zr55Cu30Al10Ni 5 metallic glass, Scr. Mater. 50 (2004) 39–44, https://doi.org/10.1016/j.scriptamat.2003.09.038.
[33] W.C. Oliver, G.M. Pharr, An improved technique for determining hardness and elastic modulus using load and displacement sensing indentation experiments, J. Mater. Res. 7 (1992) 1564–1583, https://doi.org/10.1557/JMR.1992.1564.
[34] C.A. Schuh, A.C. Lund, T.G. Nieh, New regime of homogeneous flow in the deformation map of metallic glasses: elevated temperature nanoindentation experiments and mechanistic modeling, Acta Mater. 52 (2004) 5879–5891, https://doi.org/10.1016/j.actamat.2004.09.005.
[35] A.L. Greer, Y.Q. Cheng, E. Ma, Shear bands in metallic glasses, Mater. Sci. Eng. R Rep. 74 (2013) 71–132, https://doi.org/10.1016/j.mser.2013.04.001.
[36] P. De Hey, J. Sietsma, A. Van Den Beukel, Structural disordering in amorphous Pd40Ni40P20 induced by high temperature deformation, Acta Mater. 46 (1998) 5873–5882, https://doi.org/10.1016/S1359-6454(98)00234-1.
[37] A.F. Bower, N.A. Fleck, A. Needleman, N. Ogbonna, Indentation of a power law creeping solid, Proc. R. Soc. Lond. A 441 (1993) 97–124, https://doi.org/10.1098/rspa.1993.0050.
[38] H. Li, A.H.W. Ngan, Size effects of nanoindentation creep, J. Mater. Res. 19 (2004) 513–522, https://doi.org/10.1557/jmr.2004.19.2.513.
[39] W.L. Johnson, K. Samwer, A universal criterion for plastic yielding of metallic glasses with a (T/Tg)2/3 temperature dependence, Phys. Rev. Lett. (2005) 95, https://doi.org/10.1103/PhysRevLett.95.195501.
[40] M.L. Falk, J.S. Langer, Dynamics of viscoplastic deformation in amorphous solids, Phys. Rev. Lett. 57 (1998) 14, papers2://publication/uuid/7A161E59-E63F-48C5-9E05-244363E162E1.
[41] W.P. Wu, D. Şopu, X. Yuan, O. Adjaoud, K.K. Song, J. Eckert, Atomistic understanding of creep and relaxation mechanisms of Cu64Zr36 metallic glass at different temperatures and stress levels, J. Non. Cryst. Solids (2021) 559, https://doi.org/10.1016/j.jnoncrysol.2021.120676.
[42] Z.Q. Chen, L. Huang, P. Huang, K.W. Xu, F. Wang, T.J. Lu, Clarification on shear transformation zone size and its correlation with plasticity for Zr-based bulk metallic glass in different structural states, Mater. Sci. Eng. A 677 (2016) 349–355, https://doi.org/10.1016/J.MSEA.2016.09.054.
[43] D. Pan, A. Inoue, T. Sakurai, M.W. Chen, Experimental characterization of shear transformation zones for plastic flow of bulk metallic glasses, Proc. Natl. Acad. Sci. U.S.A. 105 (2008) 14769–14772, https://doi.org/10.1073/pnas.0806051105.
[44] B.P. Sahu, A. Dutta, R. Mitra, Mechanism of negative strain rate sensitivity in metallic glass film, J. Alloy. Compd. 784 (2019) 488–499, https://doi.org/10.1016/j.jallcom.2019.01.024.
[45] A.S. Argon, Plastic deformation in metallic glasses, Acta Metallurgica 27 (1) (1979) 47–58, https://doi.org/10.1016/0001-6160(79)90055-5.
[46] F. Spaepen, A microscopic mechanism for steady state inhomogeneous flow in metallic glasses, Acta Metall 25 (1977) 407–415, https://doi.org/10.1016/0001-6160(77)90232-2.
[47] Y.J. Li, J. Mueller, H.W. Höppel, M. Göken, W. Blum, Deformation kinetics of nanocrystalline nickel, Acta Mater. 55 (2007) 5708–5717, https://doi.org/10.1016/j.actamat.2007.06.036.
[48] C. Wang, Q.P. Cao, X.D. Wang, D.X. Zhang, S.X. Qu, J.Z. Jiang, Time-dependent shear transformation zone in thin film metallic glasses revealed by nanoindentation creep, J. Alloy. Compd. 696 (2017) 239–245, https://doi.org/10.1016/j.jallcom.2016.11.264.
[49] Z.Y. Ding, Y.X. Song, Y. Ma, X.W. Huang, T.H. Zhang, Nanoindentation investigation on the size-dependent creep behavior in a zr-cu-ag-al bulk metallic glass, Metals 9 (2019), https://doi.org/10.3390/met9050613 (Basel).
[50] Y. Ma, J.H. Ye, G.J. Peng, D.H. Wen, T.H. Zhang, Nanoindentation study of size effect on shear transformation zone size in a Ni–Nb metallic glass, Mater. Sci. Eng. A 627 (2015) 153–160, https://doi.org/10.1016/j.msea.2015.01.001.
[51] Y.M. Wang, M. Zhang, L. Liu, Mechanical annealing in the homogeneous deformation of bulk metallic glass under elastostatic compression, Scr. Mater. 102 (2015) 67–70, https://doi.org/10.1016/j.scriptamat.2015.02.015.